

70%

X-520-62-92

N64 123994

Code 1

TMX-51027

(NASA-X-520-62-92, NASA
OTS: \$6.60 ph, \$2.09 mf)

63p

PLANS OFFICE TECHNICAL REPORT NO. 2

ATTENUATION IN RE-ENTRY COMMUNICATIONS

PREPARED BY
F. J. TISCHER

JUNE 19, 1962 63p ref



Comp. Auth: NASA

GODDARD SPACE FLIGHT CENTER,
GREENBELT, MD.

OTS PRICE

XEROX	\$	6.60 ph
MICROFILM	\$	2.09 mf

ROT-9595

LIST OF SYMBOLS^{1/}

A	=	Altitude
A ₀	=	Avogadro's number = 6.025×10^{23} particles/mole
B	=	Indicates dependence on body shape
C	=	Particle concentration
C _p	=	Molar heat capacity of the ith particle species
D	=	Diameter of re-entry body
\bar{E}	=	Electric field intensity
eV	=	Electron
F	=	$F_1 F_2 F_3$ Geometry factor for the electron density
G	=	$G_1 G_2 G_3$ Geometry factor for the collision frequency
f	=	Frequency
f _p	=	Plasma frequency
f ₁	=	$\log_{10} F_1$; $g_1 = \log_{10} G_1$
\bar{H}	=	Magnetic field intensity
h	=	Heat of the ith reaction
\hat{i}	=	Unit vector
\bar{J}	=	Current density representing a radiation source
j	=	$\sqrt{-1}$
K ₁	=	Equilibrium constant for the ith reaction
k _d	=	Dissociation rate constant
k _r	=	Re-combination rate constant

^{1/} The equations are written in such a form that arbitrary units can be used in consistency with the units given in the List of Symbols.

SUMMARY

12399

Methods are presented for computing the approximate attenuation of radio signals passing through the shock layer of large re-entry vehicles.

A review of the computation methods and of the availability of data for these computations shows that approximate methods with simplifications distributed evenly over all phases of the computations represent, at present, the best approach to obtain estimates for the re-entry "blackout". Based on this concept, approximate equations are derived for the re-entry attenuation. The derived equations are then applied to the MA-6 Mercury flight.

AUTHOR

k	=	Boltzmann's constant = 1.38×10^{-23} Joules/ $^{\circ}\text{K}$
L_0	=	Loschmidt number 2.687×10^{19} particles/ cm^3
M_0	=	Average molecular weight
M_e	=	Mass of one electron = 9.107×10^{-31} Kg
N_e	=	Electron density/ cm^3
N_s	=	Electron density behind normal shock
N_i	=	Particle density of the i th species
n	=	Index of refraction
P	=	Pressure
p	=	ω_p/ω normalized plasma frequency
Q	=	Collision cross-section
q	=	ν/ω normalized collision frequency
q_e	=	Charge of one electron = -1.602×10^{-19} coulomb
R_0	=	Gas constant = 1.987 cal/mole $^{\circ}\text{K}$
S	=	Entropy
T	=	Temperature in $^{\circ}\text{K}$ ($=5/9^{\circ}$ Rankine)
t	=	Time
\bar{V}	=	Velocity
$\langle v_e \rangle$	=	Average electron velocity
α	=	Attenuation constant
β	=	Phase constant
β_0	=	Phase constant for empty space

$$\Gamma = \beta - j\alpha \quad \text{complex wave propagation constant}$$
$$\mathbb{G} = \text{Dyadic Green's function}$$
$$\Delta = \text{Thickness of shock layer}$$

δ_{eq} = Equivalent plasma layer thickness

$$\epsilon_0 = \text{"Empty space permittivity"} = 8.854 \times 10^{-12} \text{ farad/meter}$$
$$\epsilon_r = \epsilon_r' - j\epsilon_r'' \text{ complex relative permittivity}$$

Λ = Collision parameter (Spitzer: Physics of Fully Ionized Gases)

$$\omega = \text{Angular frequency} = 2\pi f$$

ρ = Gas density, reflection coefficient

$$\rho_0 = \text{Normal air density} = 1.288 \times 10^{-3} \text{ gm/cm}^3$$

$$= 2.498 \times 10^{-3} \text{ slugs/ft}^3$$

τ = Complex transmission coefficient

TABLE OF CONTENTS

I.	Introduction	1
II.	Review of Subject Areas.	2
	A. Structure of the Shock Layer.	3
	B. Electrical Properties of Shocked Air.	9
	C. Medium Constants of Plasma.	11
	D. Wave Propagation Through the Shock Layer.	12
III.	Computation Method for Estimates of the Re-Entry Attenuation	17
	A. Simplified Model of the Electrical Flow- Field Properties	18
	B. Simplified Wave Propagation Model	22
IV.	Evaluation of the Mercury MA-6 Flight.	28

Appendicies:

- A. Non-Equilibrium Electron Densities in High Temperature Air
- B. Electron Density and Collision Frequency of Shocked Air
 at Equilibrium
- C. Nonuniform Wave Propagation

Attenuation in Re-Entry Communications

by

F. J. Tischer

I. Introduction:

In considering communications to and from a vehicle re-entering the atmosphere at high velocity after a space mission and attempting to compute numerical examples, one faces in the various phases of this work the following basic problem: How far should one go with the rigor and accuracy of the computations, or differently formulated, how far is one allowed to go with simplifications, approximations and neglects? It seems from a review of the few published examples that this problem is not taken properly into account. On one hand elaborate computer programs are used in certain phases of the work while in others, perhaps as important, rough approximations are being applied simultaneously.

It is the purpose of this report to review the state of knowledge and the computation methods in the various subject areas involved in re-entry communications from this viewpoint and to develop simplified computation procedures for estimates of attenuation and blackout conditions at re-entry with approximations evenly distributed over all phases.

In the main sections of this study, the problems, particularly the computation methods, are treated in a rather sketchy manner dictated by the great number of subject areas involved. They are supplemented by more detailed treatments in the various appendices. The first part contains the review of typical computation methods in the various phases of solving this communications problem. The second part deals with the derivation of the computation model, and in the third part, this model is applied to the Mercury flight, MA-6.

II. Review of Subject Areas:

The consideration of transmitting signals through the plasma layer about the body re-entering the atmosphere at high speeds can be divided up into two parts: First, the determination of the electrical properties of the plasma layer surrounding the vehicle as the result of aerodynamic heating and second, the actual wave propagation problem.

In dealing with the first problem, we can describe the electrical properties in the plasma layer by a relative permittivity ϵ_r' and a conductivity σ , or combining both, in a simpler form by a complex relative permittivity $\epsilon_r = \epsilon_r' - j\epsilon_r''$ as a single quantity. With these quantities or this quantity known, we can then compute the propagation problem by conventional methods.

A. Structure of the Shock Layer

The electromagnetic medium properties and ϵ_r depend mainly on the aerodynamic and thermodynamic characteristics of the highly non-uniform shock layer. The shock layer, structurally, is a flow field. Large variations of temperature, density, and composition are encountered in the various regions. The varying ambient air data along the trajectory of the vehicle as initial conditions complicate additionally the computations. At present, considerable efforts are being made to develop improved computation methods and programs for analyses of the structure of the shock layer by including non-equilibrium effects and transport phenomena. These considerations, unfortunately, complicate the computations to such an extent that the introduction of simplifications and neglects represents one of the primary problems as outlined previously.

For the purpose of analyzing the structure of the shock layer, we can subdivide the layer into regions which have distinctly different properties and for which different computation methods have to be used. The main region of the layer consists of an approximately inviscid flow field which is bound outside by the shock front and toward the body by a viscous boundary layer. The stagnation region in front of the body, the flow field surrounding the body, the expansion region along the after-body and the wake are the main regions.

In discussing the flow field, the simplest model is based on the thermodynamically perfect gas with a frozen composition. The next step toward a more realistic approach is to consider real gas including ionization but with chemical and thermodynamic equilibrium. With this assumption, the reaction rates are infinite. The next step of increased sophistication, with considerable efforts spent for it, is to permit local thermodynamic non-equilibrium and using finite reaction rates of the physico-chemical reactions. To include these effects in the computation brings on enormous difficulties compounded by a lack of accurate data which makes the practical usefulness of such sophisticated models questionable. It should be noted, however, that more rigorous computations are necessary to further the understanding of the basic physics of the plasma phenomena. The received data will be necessary in future computations.

At present the flow fields are usually computed on the basis of a gas in thermodynamic equilibrium with the non-equilibrium effects and the viscosity and the effect of the boundary layer introduced as a perturbation of the original field.

This solution of the equilibrium problem starts with the fundamental flow equations for an ideal gas

$$\rho \frac{d\bar{v}}{dt} = - \nabla P,$$

$$\nabla \cdot (\rho \bar{v}) = 0,$$

$$\frac{dS}{dt} = 0,$$

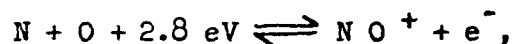
$$P = Z \rho R_c T.$$

Results of equilibrium analyses for specific forms of bodies, usually shapes composed of spheres and cylinders or cones, for specified altitudes and velocities can be found in the literature (1 to 5).

A comparative study of flow field characteristics under equilibrium conditions was published by Ridyard (6).

The assumption of equilibrium presupposes that the relaxation times of the thermo-chemical effects are small compared with the travel times of the particles. At high velocities and small body dimensions, this assumption is certainly no longer valid. This becomes particularly important in computing the electromagnetic properties of the shock layer where ionization and recombination affects considerably the electron density and hence the propagation properties.

The primary electron-forming and electron-eliminating two-way reaction is



which in turn depends on the particle densities of atomic N and O and, therefore, depends on the processes forming these particles and on the thermodynamic conditions. Direct dissociation, interchange reactions, and all the other chemical reactions are therefore important (7 to 10). Since practical computation programs can include only a limited number

of reactions, the selection and consideration of those reactions which are important seems to be one of the main problems. Herewith, the errors introduced by the neglects have to be known and of acceptable magnitude. Bortner (11) gives an account of the various reaction rates and shows the effects of different combinations of reactions.

Figure 1 (from 11) presents the results in graphical form. The diagram shows the electron density of a plasma as a function of the available reaction time considering the four most important reactions indicated in the figure. The terminal state is represented by air at equilibrium conditions behind a normal shock at 76 KM (250 Kft) altitude and 7.6 KM/Sec (25 Kft/Second) velocity. Combining these data with the travel times of particles along streamlines in the flow field gives an indication whether or not equilibrium computations are permissible. Also, the approximate errors for travel times smaller than the transition period T (see Figure 1) can be estimated.

Applying these data and the results of experiments of shock wave diagnostics using microwaves (AVCO Everett, Res. Rep. 105) to a re-entering Mercury vehicle with a velocity of approximately 6.1 KM/Sec (20 Kft/Sec) and distances of approximately 1 meter (3 feet) from the stagnation region to the shoulder of the vehicle around which the air has to flow, and with the same distance from the shoulder to the propagation point to and from

the (C-band) antenna, we find a time of approximately 1.6×10^{-4} seconds which is large compared with the relaxation time T in Figure 1. Consideration of flow fields in thermodynamic equilibrium seems hence an acceptable approximation in computations involving the Mercury capsule or vehicles of similar sizes.

Heretofore, the flow fields were considered under the assumption of a thin boundary layer which can be treated separately and introduced in the computation as a perturbation with eventual re-calculation of the inviscid flow field based on boundary conditions modified by the boundary layer. This procedure becomes, however, unrealistic in the case of high altitude conditions where the influence of viscosity and of transport phenomena and hence the boundary layer extend over a considerable part of the shock layer.

The preceding considerations were based on the assumption of uncontaminated air. In realistic and rigorous considerations, the effects of ablation and related phenomena have to be taken into account (19 to 22). The effect of contaminants and additives is important in communications also for other reasons. Such effects represent one way of how to affect artificially the electromagnetic properties of the plasma layer for improving communications. Cooling effects (19) changes of the chemical reaction rates (22) by contaminants, injection of electro-negative ions and other effects are of interest and are at present under investigation.

In the case of body shapes typical for manned space missions, the propagation path along which the signal-carrying waves travel, contains regions of separated flow which have properties similar to those in the near-wake. Several articles dealing with the properties of the wake are listed in the bibliography (15 to 18).

Surveying this rather sketchy review of the status of flow field calculations, one obtains the definite impression that an accurate computation of the flow field data, at present, is not possible because of the lack of basic information (accurate data of reaction rates, particularly with contaminants, effects of transport phenomena and viscosity, flow fields in expansion regions and near-wake, and separated-flow data).

This situation suggests that approximate computation methods making the best possible use of available data, and introducing simplified assumptions and approximations uniformly distributed in the various phases of the computation seems, at present, to be the best approach in computing the overall effect of re-entry on the signal transmission.

With this basic conclusion as background, the computation of the electromagnetic properties and the wave propagation are considered in the following sections. Simplifications are introduced wherever possible, but rigorous formulations are considered briefly also which may be of interest in more accurate calculations in the future.

B. Electrical Properties of Shocked Air

The first step in computing the passive electrical properties of the ionized air in the shock layer consists in the determination of the electron density and collision frequency as a function of the location within the layer. These quantities can be computed from the average particle density of the various constituents and their temperatures. For thermal and chemical equilibrium, these data can be computed for specific operational conditions, namely altitude and velocity according to well-established principles of thermodynamic and physical chemistry and quantum theory. The equations by which the various microscopic quantities such as particle densities N , pressure P , and temperature T are inter-related are shown in Appendix B. The electron density N_e is then given by

$$N_e = \frac{\rho}{\rho_0} L_0 C_e , \quad (1)$$

and

$$C_e^2 \approx \sum_n K_n C_i^+ , \quad (2)$$

where ρ/ρ_0 is the mass density ratio of air, L_0 the Loschmidt number, and where C_i represents the particle concentration of the i th species. The quantity K_n is the equilibrium constant for the n th ionization process.

Tables are available for the electron density and the other data for hot air at equilibrium as a function of temperature T and density ratio ρ/ρ_0 . Since these latter data also are known for air after it has passed through a normal shock front at various operational conditions (altitudes and velocities), combination of both yields the electron density under these conditions. Figure 2 shows a graph of these data published by Sisco and Fiskin (27).

The second quantity required for the description of the medium properties of the plasma layer is the electron collision frequency. This quantity, as an approximation, is the sum of contributions resulting from collisions with electrons, positive ions and the various types of neutral particles

$$\nu_{tot} = \nu_e + \nu_i + \langle v_e \rangle \sum_i N_i Q_i, \quad (3)$$

where ν_e and ν_i are the contribution by the collisions with electrons and ions respectively, and where N_i and Q_i are the particle density and collision cross-section of the i th neutral particle species respectively. A comparison of the contributions by the various particle species shows that the contributions by elastic collisions by the electrons as well as those by the ions can be neglected in approximate computations up to 6000°K. In this temperature range the main contribution results from elastic collisions

with neutral particles. The neutral particles causing collisions are the molecules and atoms, N_2 , O_2 , NO , and N , and O . The values for the cross-sections reported by various investigators differ considerably so that accurate calculations seem not possible at present. A detailed listing of the values available in the literature was published by Bachynski and co-workers (30). Figure 3 shows in diagram form averaged values of the cross-sections extracted from the literature, which can be used in combination with diagrams for the particle densities N_1 by Sisco and Fiskin (27) in air as a function of temperature $T^{\circ}K$ and density ratio ρ/ρ_0 for computing the collision frequency.

C. Medium Constants of Plasma

The electrical properties of plasma can be described simplest by a complex permittivity (42) writing

$$\epsilon = \epsilon_0 \epsilon_r = \epsilon_0 (\epsilon_r' - j \epsilon_r'') . \quad (4)$$

Assumption of a Boltzmann-Maxwell velocity distribution and a constant collision frequency permits evaluation of the integral in

$$\epsilon_r = 1 + j \frac{4\pi}{3} \frac{q_e^2}{m_e \epsilon_0} \int_v \frac{v^3 \frac{\partial f_0}{\partial v}}{\omega(j\omega + \nu)} dv, \quad (5)$$

where

$$\int_v v^3 \frac{\partial f_0}{\partial v} dv = - \frac{3}{4\pi} N_e ,$$

and yields

$$\epsilon_r = 1 - \frac{p^2}{1+q^2} - j q \frac{p^2}{1+q^2} . \quad (6)$$

In Eq. (6), $p = \omega_p/\omega$ denotes the angular plasma frequency normalized with respect to the operational frequency ω , where

$$\omega_p^2 = N_e q_e^2 / m_e \epsilon_0 .$$

The parameter q represents the normalized collision frequency ($=\nu/\omega$).

It is noted that ϵ_r is related to the index of refraction by $n = \sqrt{\epsilon_r}$.

D. Wave Propagation Through the Shock Layer

With the above medium constants, we can describe the propagation of plane waves in a uniform medium. We write for the electric field intensity

$$\vec{E} = \vec{E}_0 \exp j(\omega t - \vec{\Gamma} \cdot \vec{r}) , \quad (7)$$

where $\vec{\Gamma}$ is the propagation vector with the angle indicating the direction of wave propagation and with its magnitude,

$$\Gamma = \beta - j\alpha , \quad (8)$$

representing the complex propagation constant. Substituting the complex permittivity, we find

$$\Gamma = \sqrt{\epsilon_r} \beta_0 . \quad (9)$$

Combination of Eqs. (7), (8), and (9) and normalization yield

$$\beta' - j\alpha' = \frac{\beta}{\beta_0} - j \frac{\alpha}{\beta_0} = \left(1 - \frac{p^2}{1+q^2} - j q \frac{p^2}{1+q^2} \right)^{1/2} \quad (10)$$

The quantities β' and α' are the phase and attenuation constants normalized with respect to the phase constant for empty space β_0 . Evaluation of Eq. (10) gives for these quantities

$$\beta'^2 = \left[\sqrt{(s-1)^2 + (qs)^2} + (1-s) \right] / 2, \quad (11)$$

$$\alpha'^2 = \left[\sqrt{(s-1)^2 + (qs)^2} - (1-s) \right] / 2, \quad (12)$$

where $s = p^2/(1 + q^2)$.

Reflections at a sharp boundary between plasma and empty space can be taken into account by a complex reflection coefficient which is

$$\rho = (1 - \sqrt{\epsilon_r}) / (1 + \sqrt{\epsilon_r}).$$

With this quantity, we obtain as the relative power transmitted through the discontinuity at the boundary

$$|\tau|^2 = \left[(1 + \beta'^2) - (1 - \beta'^2) \right] / \left[(1 + \beta'^2) + \alpha'^2 \right]. \quad (13)$$

Eventually, the reflections can be taken into account by a logarithmic attenuation factor where

$$R_{\text{refl}} \text{ in DB} = 8.686 \ln |\tau|^2.$$

The computations involving the attenuation and phase constants can be considerably simplified by the introduction of approximate equations which are valid in particular regions of the values of these quantities. Usually, at high altitudes the normalized collision frequency is small ($q \ll 1$). Under these conditions, and distinguishing between two regions for p , one for $p < 0.5$, and one for $p > 1.5$, we find:

$$\begin{aligned} q \ll 1, \quad p < 0.5 : \alpha' &\approx \frac{1}{2} p^2 q, \\ p > 1.5 : \alpha' &\approx \sqrt{p^2 - 1}, \\ p > 3 : \alpha' &\approx p. \end{aligned} \quad (14)$$

In the transition region, when $0.5 < p < 1.5$, α' depends considerably on the collision term. We find:

$$\begin{aligned} p = 0 : \alpha' &\approx \frac{1}{2} q^2, \\ p = \frac{1}{2} q^2 : \alpha' &\approx \sqrt{q/2}. \end{aligned}$$

In this region the rigorous Eq. (12) has to be used for the computation of the attenuation.

In considering the actual wave propagation through the plasma layer, the nonuniformity of the medium has to be taken into account. The

following method described in the literature (35) can be used. The method is based on a successive approximation, where the field intensity is written as an asymptotic series

$$\bar{E}(\bar{r}) = \bar{E}_0 + \sum_{n=1}^{\infty} \Delta \bar{E}_n(\bar{r}) \quad (15)$$

The first term results from radiation in a uniform medium with average medium constants. The following terms represent the deviations from the first-term intensity. For the deviations, a recursion formula can be derived, which is

$$\Delta \bar{E}_n = \int_V \bar{\Gamma}(\bar{r}, \bar{r}') \cdot \left\{ j \frac{\omega \epsilon_0}{\beta_0} \nabla \left[\frac{\nabla \epsilon_r(\bar{r}') \cdot \Delta \bar{E}_{n-1}}{\epsilon_r(\bar{r}')} \right] + j \omega \epsilon_0 [\Delta \epsilon_r(\bar{r}') \Delta \bar{E}_{n-1}] \right\} dV \quad (16)$$

The method is outlined in more detail in Appendix C.

The described method has the advantage that approximations of arbitrary degrees of accuracy can be derived by neglecting higher order terms and choosing an appropriate coordinate system.

A drastic simplification is obtained by considering layers with the medium stratified in the direction of one coordinate only. The resulting first order approximation is then, assuming plane waves,

$$\bar{E}_0(z, t) = \hat{i}_x \exp[j(\omega t - \beta_0 z)], \quad (17)$$

entering a layer with a relative permittivity

$$\epsilon_r(\bar{r}') = 1 + \Delta\epsilon_r(z') ,$$

$$\bar{E} \approx \hat{i}_x \exp j\omega t \exp(-j\beta_0 z) \exp\left(\int -j \frac{\beta_0}{2} \Delta\epsilon_r dz\right) .$$

We write for the complex permittivity which does not deviate strongly from one

$$\sqrt{\epsilon_r} \approx 1 + \frac{1}{2} \Delta\epsilon_r' - \frac{1}{2} j \Delta\epsilon_r'' \approx \frac{\beta}{\beta_0} - j \frac{\alpha}{\beta_0} .$$

We obtain finally

$$|E| = \exp\left(-\int_0^z \alpha_\epsilon dz\right) , \quad (18)$$

where the integral represents the attenuation in Nepers. The total attenuation in DB is

$$R_0^{DB} = 8.686 \int_0^z \alpha_\epsilon dz . \quad (19)$$

This quantity can be corrected by terms ΔR_y , if greater accuracy is desired. We obtain

$$R_{tot}^{DB} = R_0 + \sum_y \Delta R_y ,$$

where the additional terms may take into account the geometry of

radiation, the antenna structure, reflections, and other effects. These terms can be derived from the higher order terms of Eq. (15).

Equation (19) also shows that the reflections in media with slowly varying medium constants can be neglected. These conditions are fulfilled in the case of large vehicles typical for manned space flight which also usually are surrounded by thick shock layers. The conclusions which have to be drawn from this review are not in favor of accurate computations. Such computations in which most of the important flow-field and propagation phenomena are taken into account, involve so many parameters that a solution is almost impossible. Differences of experimentally obtained data necessary in the computations and published by different investigators also decreases the value of accurate computations.

III. Computation Method for Estimates of the Re-Entry Attenuation:

The preceding review of the subject areas involved in re-entry communications shows that approximate methods for estimates of the effect of the plasma layer on the signal transmission seems to represent the most appropriate approach in solving this problem at present. Here-with, it is desirable to distribute the simplifying approximations uniformly over all phases of the computation. Development of an approximate computation procedure is the subject of the following sections.

The computation of re-entry communications can be divided up into two parts: First, the distribution of the electron density and collision frequency is determined as a function of the position within the shock layer. Then, the wave propagation problem is treated in a conventional manner applying the data obtained in Part 1.

A. Simplified Model of the Electrical Flow-Field Properties

The first part involves the electric characteristics of the flow field. Since the computation of flow-field data with desirable accuracy, at present, is almost impossible, we express the electron density and collision frequency without knowing the actual structure of the flow field in a generally valid form as follows:

$$N_e = N_s(A, V) F\left(\frac{x}{D}, \frac{y}{\Delta}, A, V, B, \dots\right), \quad (20)$$

$$\nu = \nu_s(A, V) G\left(\frac{x}{D}, \frac{y}{\Delta}, A, V, B, \dots\right). \quad (21)$$

The various quantities in these equations are:

N_e, ν . . . Electron density and collision frequency
in an arbitrary point of observation
within the shock layer.

N_s, ν_s . . . The same quantities behind a normal shock
at an altitude A and a velocity V .

- x/D . . The distance along a near-body streamline normalized with regard to the body diameter.
- y/Δ . . Distance from body to the point of observation across streamlines normalized with regard to shock layer thickness Δ .
- F G . . Functions of x/D , y/Δ , A, V, and B which indicates the body shape, and of other parameters.

We search next for approximate functions for F and G using the thermodynamic and electric characteristics of flow-field examples published in the literature (5, 6). The available data are those of flow-fields around shapes composed of spheres, cones, and cylinders. Figure 4 shows typical distributions of the electron densities and collision frequencies across the shock layer at the position A and B obtained by evaluation of data from the literature. The diagrams are typical and suggest the approximate representation of the electron density and collision frequency by the following functions: an exponential function for the electron density, while the collision frequency can be expressed by a constant. Since the basic form of the electron distribution is similar for different values of x/D , we apply a product presentation of F and write

$$F \approx F_1 (x/D) F_2 (y/\Delta) F_3 (x/D, y/\Delta, \text{material}), \quad (22)$$

where

$$F_2 (y/\Delta) = \exp [-k (y/\Delta)^2] . \quad (23)$$

The function F_1 describes the variation of the electron density along a near-body streamline, where the electron density is approximately a maximum, F_2 represents the variation across streamlines in direction of wave propagation and F_3 is a correction factor which takes into account eventual effects of ablating materials.

Similarly, we write for the distribution of the collision frequency

$$G = G_1(x/D) G_2(y/\Delta) G_3(x/D, y/\Delta, \text{material}), \quad (24)$$

and we assume for G_2 unity.

With these assumptions, we find for the electrical data within the shock layer

$$N_e' = N_s F_1(x/D) F_3 \exp [-k (y/\Delta)^2], \quad (25)$$

$$\nu = \nu_s G_1(x/D) G_3. \quad (26)$$

The next step is to investigate $F_1(x/D)$ and $G_1(x/D)$ which describe the variations of the maximum of the electron density and of the collision frequency along a near-body streamline. Figure 5 shows the longitudinal distributions for the same example (with the geometry indicated in Figure 4). We observe large variations over powers of magnitude of N_e and considerably smaller variations of ν_e . It seems hence useful to express F_1 and G_1 by logarithmic functions so that

$$\log_{10} F_1 = f_1(x/D)$$

and

$$\log_{10} G_1 = g_1(x/D).$$

Since the function of f_1 and g_1 depend considerably on the body shape, we do not introduce any particular functions. It is noted, however, that for a given position of the antenna along the body, the values F_1 and G_1 or f_1 and g_1 are constant for a given altitude and velocity. Their magnitudes have to be determined by flow-field calculations or in real-flight experiments.

The question arises now as to which extent the functions F_1 and G_1 are affected by changes of altitude and velocity. Exploration of published data (40, 5, 6) shows that the deviation of the longitudinal distribution functions are relatively small in the region from 25 to 80 KM

(75 to 250 KFT) altitude. This means that the above approximate presentation by constant geometry factors F_1 and G_1 describes satisfactorily the electrical properties of the shock layer along the afterbody behind $x = D/2$ during the re-entry blackout which occurs usually in the region between the above altitudes.

B. Simplified Wave Propagation Model

In this second part dealing with the wave propagation problem, we have, as a first step, to substitute the electrical flow-field data represented by Eqs. (25) and (26) into the equation for the medium constant for the transmission medium, namely the complex permittivity of the plasma. These data, in turn, yield the complex propagation constant consisting of the phase and attenuation constants as a function of the position within the shock layer. Using the equations of sections B and C of Part II, we find

$$p = \omega_p / \omega = 56.5 \times 10^3 \sqrt{N_e} / \omega ,$$
$$q = \nu / \omega ,$$

which, introduced in Eq. (6) give the corresponding permittivity.

The attenuation of the signal and, consequently, the attenuation constant are of primary interest in the case of the communications

"blackout". For the determination of this quantity, we apply the approximate equations derived in section D of Part II.

An indication of the regions of validity of these equations seems to be appropriate at this point. The equations are valid in the case of large-size vehicles, if the lengths of the transmission path within the shock layer is long compared with the wavelength and when the plasma is under-dense to the time when the attenuation reaches "blackout" values. Since these conditions are fulfilled in our case, we can use Eq. (19) so that

$$\alpha' = \alpha / \beta_0 \approx p^2 q / 2 = 1.6 \times 10^9 N_e \nu / \omega^3 ,$$

and

$$\alpha \approx K_1 N_e \nu , \quad K_1 = 1.6 \times 10^9 \beta_0 / \omega^3 , \quad (27)$$

where K_1 includes the various constant quantities. Substituting into the equation for the total attenuation, we find

$$R_{tot} \approx 8.7 K_1 \int_0^{\Delta} N_e \nu dy , \quad (28)$$

integrated along the transmission path within the plasma. The result can be interpreted as follows: The total attenuation is proportional to the total electron content in a tube of one square centimeter

cross-section through the shock layer along the transmission path, the collision frequency being within the shock layer as an approximation constant. This result is in agreement with the relations typical for ionospheric diagnostics where measured ionospheric effects usually yield the total electron content in a column of unit area along the transmission path. Substituting into Eq. (28) the relations for the electrical flow-field characteristics, we obtain

$$R_{\text{tot}}^{\text{DB}} \approx 8.7 K_1 N_5 v_5 F_1 F_3 G_1 G_3 \int_0^{\infty} \exp[-k(y/\Delta)^2] dy, \quad (29)$$

where the integral was extended to infinity. The extension to infinity is permissible since the shock layers have in most practical cases such a thickness that the electron density has decayed at the oblique shock front by several orders of magnitude. The contribution by the exponential function for $y \gg \Delta$ is hence negligible.

Evaluation of the integral which has the basic form

$$\int_0^{\infty} \exp(-\lambda/y^2) dy = \sqrt{\pi/\lambda}/2$$

yields

$$\int dy = \Delta \sqrt{\pi/k}/2.$$

The next step is to substitute useful quantities for Δ and k . In

analogy with skin depth considerations in electromagnetics, we introduce a so-called equivalent shock-layer thickness δ_{eq} , which represents the thickness of a uniform plasma layer which gives the same attenuation as the actual nonuniform sheath. With this quantity, the integral Eq. (29) becomes δ_{eq} , so that

$$F_2(y/\Delta) = \exp[-k(y/\Delta)^2] = \exp[-0.79(y/\delta_{eq})^2]. \quad (30)$$

From practical viewpoints δ_{eq} is not very useful since the decrease ($1/e$) of the electron density at this distance from the body is too small to give sufficient accuracy in our considerations. The shock layer thickness Δ , on the other hand, is too large for practical purposes to permit a good approximation of the electron density distribution. As a consequence, it seems appropriate to introduce a distance L from the body along the transmission path where the electron density has decreased by 2 orders of magnitude. This definition brings L into a region for which data are available with acceptable accuracy in the literature and where the effect of deviations from the idealized exponential function near the body is greatly reduced. We note that with this definition, $\delta_{eq} = 0.467 L$.

The total attenuation in uncontaminated air and neglecting ablation is then

$$R_{tot} \approx 8.7 K_1 N_s \nu_s F_1 G_1 \delta_{eq} ,$$

and finally

$$R_{tot} \approx 8.8 \times 10^{10} N_s \nu_s F_1 G_1 (\delta_{eq} / \lambda_0) / \omega^3,$$

where λ_0 and ω are the operational wavelengths and angular frequency respectively. Re-arranged, the equation becomes

$$\boxed{R_{tot} \Big|_{\text{under-dense}} \approx 0.012 N_s \nu_s F_1 G_1 \delta_{eq} / f^2} \quad (31)$$

where N_s , ν_s are the electron density and collision frequency behind a normal shock, which take into account the variations of R_{tot} at the various positions along the trajectory, where F_1 and G_1 are flow-field geometry factors which indicate the decreases of the electron density and collision frequency along a near-body streamline in the region of maximum electron density, δ_{eq} is the equivalent shock layer thickness ($\delta_{eq} = 0.467 L$), and f is the operational frequency.

The geometry factors F_1 and G_1 , and δ_{eq} can be obtained from flow-field considerations or, they can be determined by the evaluation of attenuation measurements carried through in real flight.

Concerning the validity of Eq. (31), it should be noted that the equation can be applied during re-entry in direction toward lower altitudes down to the point shortly before the actual "blackout" starts and again, however with caution, after "blackout" when the plasma layer

becomes under-dense. After "blackout" has started, the plasma becomes over-dense and the attenuation increases very rapidly to extremely large values. In this region, we can use for the plasma characteristics the approximation Eq. (14) for $p > 3$ which yields for the total attenuation

$$R_{\text{tot}} \Big|_{\text{over-dense}} \approx 0.23 \times 10^{-4} \sqrt{N_s} \sqrt{F_1} \sqrt{F_3} \delta_{\text{eq}} . \quad (32)$$

In the transition region and when the collisions are no longer negligible, the approximate equations are inadequate and the rigorous Eq. (12) has to be applied.

In considerations dealing with the time when a re-entry vehicle enters "blackout", Eq. (32) is of minor importance. However, if the electron density is large and the shock layer contains an over-dense region, this equation becomes interesting insofar as it indicates that under these conditions the total attenuation becomes frequency independent. The reduction of the equivalent thickness δ_{eq} is then the main contributor to a decrease of the attenuation. The fact that Eq. (32) does not contain the frequency as a variable parameter needs further investigation.

Returning to Eq. (31), two problems should be noted also: One is the effect of reflections of the waves within the shock layer, the other is the effect of the boundary layer. Since the gradient of the

permittivity is small in the case of large vehicles, the effect of reflections can be neglected. Wave reflections are, under these conditions, already included in Eq. (19). For more rigorous considerations, the higher-order terms of Eq. (15) will take into account the effect of the reflections. In rigorous computations based on the plane wave approach, solutions of the wave propagation problem lead to second-order differential equations with variable coefficients. A direct solution of this equation by electronic computers may be simpler than the successive approximation method considered previously (39).

The effect of the boundary layer can be taken into account in simplified computations by reducing the equivalent plasma layer thickness δ_{eq} by the thickness of the boundary layer.

IV. Evaluation of the Mercury MA-6 Flight:

Let us apply the computation methods outlined above and Eq. (31) in considering the re-entry "blackout" of the Mercury Flight MA-6. Let us proceed, herewith, in the following manner. Since field strength data are available at several frequencies, we can use the data at one frequency for obtaining the geometry factor F_1 and G_1 and then use this factor for checking the "blackout" time at one of the other frequencies. Simultaneously, this example shows how to use Eq. (31) and how to obtain the various quantities involved. The example may also serve for further explanations.

The trajectory data from MA-6 re-entry are shown in Figure 6 by plots of altitude and velocity versus time.

Let us next re-write Eq. (31) with all variables included;

$$R_{tot} \approx 0.012 N_s(A,V) \nu_s(A,V) F_1(B, \frac{x}{D}) G_1(B, \frac{x}{D}) \delta_{eq}(B, \frac{x}{D}) / f^2 .$$

We observe that N_s , ν_s , the electron density and collision frequency behind a normal shock are functions of altitude and velocity. These quantities have to be determined and plotted for the particular re-entry trajectory, in the present case based on the data of Figure 6. Instead of plotting N_s , it is useful to substitute the corresponding plasma frequency f_{ps} which is related to N_s by $f_{ps} \approx 9 \times 10^3 \sqrt{N_s}$. Figure 7 shows plots of the plasma and collision frequencies along the trajectory versus flight time.

The geometry factor $F_1(B, x/D)$, which takes into account the reduction of the maximum electron density along the near-body streamline farther back on the body, depends mainly on the body shape and the position along the streamline. The quantities G_1 and δ_{eq} are mainly functions of the same parameters. It should be noted that for a given body shape and a fixed position of the antenna on the body, the functions F_1 , G_1 and δ_{eq} are as an approximation constants. As they are known, they can eventually be lumped together in one constant which then can be determined by real-flight experiments.

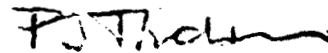
In our considerations, we use first rough estimates obtained from inspection of Figures 4 and 5. The plotted data suggest that $\log_{10} F_1 = f_1(x/D)$ for the body shape of the Mercury 6 can be assumed to be between -1 and -3. As a consequence, we assume 3 values $f_1 = -3, -2, \text{ and } -1$. For $\log_{10} G_1 = g_1(x/D)$, we choose $g_1 = -1$ which may come close to the actual value. Figure 8 shows plots for the maximum plasma frequencies $f_{p1}, f_{p2}, \text{ and } f_{p3}$ for the 3 assumed values of f_1 and the collision frequency ν_1 for $g_1 = -1$.

A rough flow-field consideration yields for the equilibrium shock layer thickness with the present geometry in position of the C-band antenna $\delta_{eq} \approx 33 \text{ cm}$.

If we now compute the attenuation for an operational frequency of 5.5 GC along the trajectory caused by the plasma sheath and plot its values as a function of time downwards from a level without plasma effects, we obtain the 3 curves shown in Figure 9 by the dotted, dash-dotted, and dash-double-dotted lines. (The attenuation in the transition region from under-dense to over-dense plasma was computed by the rigorous Eq. (12).)

Comparison with the actual measured attenuation by the radar station in San Salvatore during the MA-6 re-entry, indicated in the figure by the solid line, shows that the actual value for F_1 seems to be around -2.5.

Carrying through the same computations for the telemetry frequency 260 mc, the corresponding curves are shown in Figure 10. We observe that a somewhat larger negative value, $f_1 = -2.7$ gives the correct "blackout" time. This seems reasonable since the antennas for telemetry are located further back on the body of the MA-6 vehicle where the geometry factor shows an additional decrease of the electron density.



F. J. Fischer
Staff Member
Plans Office



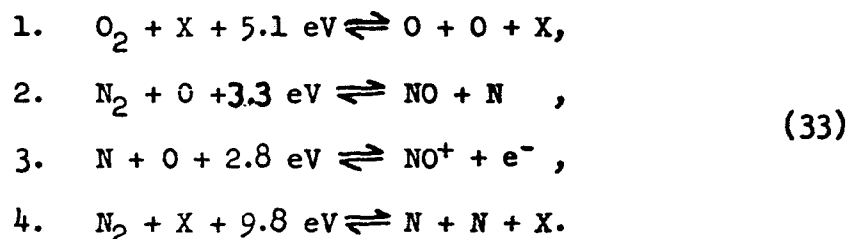
F. O. Vonbun
Head, Plans Office

APPENDIX A

Non-Equilibrium Electron Density in High Temperature Air

The gas with ambient composition and characteristics entering the shock layer in front of a re-entry vehicle is highly compressed and heated. Physico-chemical reactions take place which change the internal energy distribution and the thermodynamics of the gas and consequently also its electrical characteristics. Dissociation, ionization, and re-combination are the main contributions to the change of the characteristics of the medium in the shock layer. In rigorous flow-field computations, all the reactions have to be taken into account. At present, considerable efforts are made in studies of the various reactions and for obtaining figures for the reaction rates and cross-sections.

In considering a variety of reactions, Bortner has shown that the following four reactions yield the main contributions to the content of electrons, and are thus of particular importance in considering the interaction with electromagnetic waves. These reactions are:



The rate constants and equilibrium constants for the reactions in right-hand direction are:

$$\begin{aligned}
 k_{d1} &= 2.5 \text{ to } 25 \times 10^{+11} T^{\frac{1}{2}} (D/RT)^{1.5} \exp (-D/RT), D = 118,000; \\
 k_{d2} &= 7 \times 10^{13} \exp (-75,500/RT); \\
 k_{d3} &= 6.4 \times 10^9 T^{\frac{1}{2}} \exp (-63,290/RT); \\
 k_{d4} &= 1.7 \text{ to } 20 \times 10^{12} T^{\frac{1}{2}} (D/RT)^2 \exp (-D/RT), D = 224,900.
 \end{aligned}$$

The rate constants for re-combination k_{rv} are related to the above dissociation rates by the equilibrium constants $K_v = k_{dv}/k_{rv}$:

$$\begin{aligned}
 K_1 &= 1.2 \times 10^3 T^{-\frac{1}{2}} \exp (-D/RT) \text{ moles/cm}^3, D = 118,000, \\
 K_2 &= 4.5 \times \exp (-75,500/RT), \\
 K_3 &= 3.6 \times 10^{-2} T^{1.5} \exp (-63,290/RT), \\
 K_4 &= 18 \exp (-D/RT), D = 224,900.
 \end{aligned}$$

The electron density after a time Δt considering as an example only the number 3 reaction is then

$$N_e|_{\Delta t} = N_{e0} + \int_0^{\Delta t} \frac{dN_e}{dt} dt, \quad (34)$$

where

$$\frac{dN_e}{dt} = \frac{dN_{O^+}}{dt} = k_{d3} N_N N_O - k_{r3} N_{NO^+} N_{e^-}. \quad (35)$$

Taking into account also the other reactions (2 to 4), we have a system of six simultaneous differential equations.

Besides the composition, temperature effects have to be considered

which can be described by

$$\frac{dT}{dt} = \sum_i \frac{dN_i}{dt} h_i / \sum_j N_j c_{pj} , \quad (36)$$

where:

N_i particle density of species i reacting in reaction i ,

N_j particle density of species j ,

c_{pj} molar heat capacity of species j ,

h_i heat of reaction i ($1 \text{ eV} \approx 3.8 \times 10^{-20} \text{ cal}$).

It should be noted that Eq. (36) is coupled to the particle density equations since the rate constants for the various reactions are temperature dependent.

In considering non-equilibrium conditions, the flow field is subdivided into stream tubes bound by equilibrium streamlines, and the reactions are computed along the path of the particles within the tubes. A large number of stream tubes has to be considered due to the large gradients of the flow-field characteristics across the shock layer. In each stream tube, different conditions prevail which vary continuously with the varying input conditions according to the varying ambient data of the air along the vehicle trajectory. Taking all of these factors into account gives an indication of the complexity of the problem.

Inspection of the reaction constants shows that some of the data (k_{d1} , k_{d4}) depend largely on the type of catalyst participating in the reaction and denoted in the reaction equations by X. The presence of more than one catalyst further complicates the problem. It should also be noted that the inaccuracies in analyses and experiments involving reaction rates are considerable. The inaccuracies on one hand and the complexity of the non-equilibrium computations on the other hand make the practical usefulness of more rigorous computations, before the influences of the inaccuracies and before the effects of neglects of the various reactions are known, questionable.

APPENDIX B

Electron Density and Collision Frequency of Shocked Air at Equilibrium

The electron density N_e and the collision frequency ν are needed as parameters in the computation of the electrical properties of air. In these computations, the various physical quantities and observables are interrelated by the following equation:

$$P = \rho \frac{R_0 T}{M} \sum_i C_i, \quad (37)$$

where P is the pressure, ρ the mass density, R_0 the gas constant, M the average molecular weight, and where the constants C_i are connected to the particle densities N_i by $C_i = N_i \left(\frac{\rho}{\rho_0} L_0 \right)^{-1}$. The constant L_0 denotes the Loschmidt number and $\frac{\rho}{\rho_0}$ is the mass density ratio (see list of symbols).

The electron density is then given by

$$N_e = \frac{\rho}{\rho_0} L_0 C_{e^-}, \quad (38)$$

and C_{e^-} , as an approximation, by

$$C_{e^-}^2 \approx C_{NO^+} K_1 + C_{O^+} K_2 + C_{N^+} K_3. \quad (39)$$

The constants K_i are the equilibrium constants for the ionization processes involving NO, O, and N (given by Hochstim (20)).

Tables are available which give the values of the electron density for equilibrium air at a temperature $T^{\circ}\text{K}$ and density ratio ρ/ρ_0 as variable parameters (23 to 27).

In combination with tables for the temperature and density ratio of air after it has entered a normal shock in front of a body traveling at a specified velocity in air at a specified altitude, we obtain the electron density for these operational conditions (see Fig. 2).

It should be noted that these data also can be applied as an approximation to air after traveling through an oblique shock front using the velocity component normal to the shock front as the velocity parameter.

The other quantity required for the definition of the electrical properties of ionized air is the electron collision frequency. The total collision frequency consists of contributions by collisions with electrons, ions, and neutral particles. We can write

$$\nu_{\text{tot}} \approx \nu_e + \nu_i + \langle v_e \rangle \sum_i N_i Q_i, \quad (40)$$

where, as an approximation, the total collision frequency is the sum of the collisions with the particles of the various species. The quantities N_i and Q_i are the number density and collision cross-section of the i th species respectively, and $\langle v_e \rangle$ is the average electron velocity given by

$$\langle v_e \rangle = (8kT/\pi m_e)^{1/2}. \quad (41)$$

In Eq. (41) which is obtained assuming a Boltzmann-Maxwell velocity distribution, k is Boltzmann's constant, and m_e the mass of the electron (see list of symbols).

In approximate computations, the electron-electron collisions can be neglected due to the small mass of the electrons as deflecting particles in comparison with that of the ions. The contribution by the collisions with the ions is as an approximation

$$\nu_i \approx 2.5 \frac{N_i}{T^{3/2}} \ln \Lambda, \quad (42)$$

where Λ is a parameter which depends on electron and ion data and takes into account the collision geometry. A diagram for the determination of ν_i is shown in Fig. 11 with temperature and ion density as variable parameters for single-charged ions (Delcroix: *Theorie des Gaz Ionizés*).

Comparison of the contributions to the collision frequency by ions and neutral particles shows that, as an approximation, ion collisions can be neglected in air below a temperature of 6000°K.

The main contributors to the elastic collisions at medium temperatures are N_2 , O_2 , NO , O , and N . These contributions are taken into account by the third term of Eq. (40). The values of the collision cross-sections Q_1 , usually determined experimentally, reported by different experimentors differ considerably, particularly for atomic oxygen and

nitrogen. Accurate calculations, at present, seem impossible. Available values extracted from the literature are shown in Fig. 3. These data in combination with those of particle densities (Sisco and Fiskin (27)) permit the computation of the electron densities and the average collision frequencies dependent on the operational conditions.

APPENDIX C

Nonuniform Wave Propagation

The following method (34) considering wave propagation in a non-uniform medium based on a successive approximation has the advantage that, by neglecting higher order terms, one can choose arbitrarily the accuracy of the solution in accordance with that of the other phases of the computation. This permits considerable simplification.

We start with the vector wave equations and write

$$\nabla \times \nabla \times \bar{E} = -j\omega\mu \nabla \times \bar{H} = \omega^2 \epsilon_0 \mu_0 \epsilon_r(\bar{r}') \bar{E} - j\omega\mu \bar{J}, \quad (43)$$

$$\nabla \times \nabla \times \bar{H} = j\omega\epsilon_0 \epsilon_r(\bar{r}') \nabla \times \bar{E} + j\omega\epsilon_0 [\nabla \epsilon_r(\bar{r}') \times \bar{E}], \quad (44)$$

where

$$\epsilon_r(\bar{r}') = 1 + \Delta \epsilon_r(\bar{r}'). \quad (45)$$

The electric field intensity at a position \bar{r} is then found to be

$$\begin{aligned} \bar{E}(\bar{r}) = \int_V \bar{\bar{F}}(\bar{r}, \bar{r}') \left\{ \bar{J} + j \frac{\omega \epsilon_0}{\beta_0} \nabla \left[\frac{\nabla \epsilon_r(\bar{r}') \cdot \bar{E}(\bar{r}')}{\epsilon_r(\bar{r}')} \right] + \right. \\ \left. + j\omega\epsilon_0 [\Delta \epsilon_r(\bar{r}') \bar{E}(\bar{r}')] \right\} dV, \end{aligned} \quad (46)$$

with

$$\bar{\bar{\Gamma}} = \frac{1}{4\pi j \omega \epsilon_0} (\beta_0 \bar{\bar{\Delta}} + \nabla \nabla) \frac{\exp(-j\beta_0 |\bar{r} - \bar{r}'|)}{|\bar{r} - \bar{r}'|} \quad (47)$$

representing a dyadic Green's function.

The integral equation (46) can be solved by a method of successive approximation writing

$$\bar{E}(\bar{r}) = \bar{E}_0(\bar{r}) + \sum_{n=1}^{\infty} \Delta \bar{E}_n(\bar{r}) . \quad (48)$$

The first term results from radiation assuming a uniform medium with averaged medium constants. The following terms represent the deviations from this original value. The deviation terms are interrelated by the following recursion formula

$$\begin{aligned} \Delta \bar{E}_n = \int_V \bar{\bar{\Gamma}}(\bar{r}, \bar{r}') \left\{ j \frac{\omega \epsilon_0}{\beta_0} \nabla \left[\frac{\nabla \epsilon_r(\bar{r}') \cdot \Delta \bar{E}_{n-1}}{\epsilon_r(\bar{r}')} + \right. \right. \\ \left. \left. + j \omega \epsilon_0 [\Delta \epsilon_r(\bar{r}') \Delta \bar{E}_{n-1}] \right\} dV \end{aligned} \quad (49)$$

If the dimensions of the radiating structure and of the nonhomogeneities are large compared with the wavelength, we can assume, as an approximation, a one-dimensional stratification (plane wave case) and we write for the waves traveling in the Z-direction

$$\bar{E}_0(z, t) = \hat{i}_z \exp[j(\omega t - \beta_0 z)] . \quad (50)$$

The first order approximation yields

$$\bar{E} = \hat{i}_x \exp j\omega t \exp(-j\beta_0 z) \exp\left(-j \frac{\beta_0}{2} \int \Delta \epsilon_r(z) dz\right). \quad (51)$$

We write for the complex permittivity which does not strongly deviate from one

$$\sqrt{\epsilon_r} = \sqrt{1 + \Delta \epsilon_r} = \sqrt{1 + \Delta \epsilon_r' - j \Delta \epsilon_r''} \approx 1 + \frac{1}{2} \Delta \epsilon_r' - j \frac{1}{2} \Delta \epsilon_r'',$$

and introduce the phase and attenuation constants

$$\pm \sqrt{\epsilon_r} = \frac{\beta}{\beta_0} - j \frac{\alpha}{\beta_0}$$

so that finally

$$|E| \approx \exp\left(-\int_0^z \alpha_\epsilon dz\right), \quad (52)$$

which is in agreement with the familiar equation for the attenuation R in a medium with slowly varying medium parameters:

$$R \text{ Nepers} \approx \int_0^z \alpha \text{ Nepers/m} dz. \quad (53)$$

This approximation is being applied in section B of Part III.

BIBLIOGRAPHY

1. Hayes, W. D. and Probst, R. F.: Hypersonic Flow Theory, Academic Press, New York, N. Y., 1959
2. Gravelos, F. G., et al: The Supersonic Flow About a Blunt Body of Revolution for Gases at Chemical Equilibrium, Proc. 9th Int. Astronautical Congress, Amsterdam 1958, pp 312-332, Springer Verlag, Wien, 1959.
3. Probst, R. F. : Shock Wave and Flow Field Development in Hypersonic Re-entry. ARS J., Vol. , pp 185-194, Feb. 1961
4. Feldman, S.: Trails of Axis-Symmetric Hypersonic Blunt Bodies Flying through the Atmosphere. AVCO Corp. Res. Rep. No. 82, 1959
5. General Electric, Space Sciences Lab., Philadelphia, Pa.: Investigation of Interference Effects upon High Thrust Piloted and Pilotless Vehicular Electronic System Performance, WADD Techn. Rept. 61-191.
6. Ridyard, H. W. : Comparison of the Ionized Shock Layer about Two and Three Dimensional Blunt Shapes at Hypersonic Speeds. Electromagnetic Effects of Re-Entry, Pergamon Press, New York, 1961
7. Shkarofsky, I. P. et al: Relaxation Phenomena in Shock Fronts, Proc. of Symp. on Plasma Sheath, U. S. Dept. of Commerce, Wash., D. C., 1-59, Dec. 1959
8. Hansen, C. F. and Heims, S.P.: A Review of the Thermodynamic, Transport and Chemical Reaction Rate Properties at High Temperature Air, NACA TN 4359, July 1958
9. Bortner, M. H.: The Effect of Errors in Rate Constants on Non-Equilibrium Shock Layer Electron Density Calculations, Electromagnetic Effects of Re-entry, Pergamon Press, 74-78, 1961.
10. Lin, S. C.: Rate of Ionization Behind Shock Waves in Air, Pergamon Press, 94-99, 1961.
11. Bortner, M. H. : A Method for the Calculation of Non-Equilibrium Electron Densities in High Temperature Air, General Electric, MSVD, TIS-R61SD022, Feb. 1961

12. Wray, K. L. : Chemical Kinetics of High Temperature Air. AVCO Corp., Everett, Mass., Res. Rep. 104, Jun 1961
13. Probstein, R. F. and Kemp, N. H.: Viscous Aerodynamic Characteristics in Hypersonic Rarified Gas Flow, IAS Rep. No. 56-62, Jan. 1959
14. Scala, S. M.: On the Hypersonic Viscous Shock Layer, ARS Jol. Vol. 29, 520-526, 1959
15. Chapman, D.R.: A Theoretical Analysis of Heat Transfer in Regions of Separated Flow. NACA TN 3792, 1956
16. Chapman, D. R. et al: Investigation of Separated Flows in Supersonic and Subsonic Streams with Emphasis on the Effect of Transition, NACA TN 3869, 1957
17. Lin, S. C.: Ionized Wakes of Re-Entry Objects, AVCO Everett Res. Lab. Rep. No. 131, 1959
18. Ting, L. and Libby, P. A.: Fluid Mechanics of Axis-Symmetric Wakes behind Bodies in Hypersonic Flow, General Applied Science Lab., Techn. Rep. No. 145 1960
19. Scala, S. M. and Videle, G.: Vaporization Processes in the Hypersonic Laminar Boundary Layer, GE, TIS-Rep. Z59SD323, 1959
20. Hochstim, A. R.: Electron Concentration in Closed Form for High-Temperature Air and Air with Additives, Pergamon Press, 79-93, 1961
21. Betchov, R., et al: Modification of the Electrical Properties of the Plasma Sheath by Contaminant Injection, Aerospace Corp., Rept. No. TDR-930(2230-03) TN-6, March 1962
22. Kuhns, P. W.: Effects of Addition of Impurities on Electron-Ion Recombination Times and on Transmission Through Ionized Layers,
23. Gilmore, F. R.: Equilibrium Composition and Thermodynamic Properties of Air to 24,000°K, Rand Corporation, Rep. RM-1543, August 1955.
24. Logan, J. G.: The Calculation of the Thermodynamic Properties of Air at High Temperatures, Cornell Aeronautical Laboratory, Rep. AD-1052-A1 May 1956, Rep. BE-1007-A3 Jan 1957
25. Huber, P. W.: Tables and Graphs of Normal Shock Parameters at Hypersonic Mach Numbers and Selected Altitudes, NACA TN 4352, 1958

26. Feldman, S.: Hypersonic Gas Dynamic Charts for Equilibrium Air, AVCO Res. Lab., Jan. 1957.
27. Sisco, W. B. and Fiskin, J. B.: Basic Hypersonic Plasma Data of Equilibrium Air for Electromagnetic and Other Requirements. In same as (9), 47-73, 1961
28. Tischer, F. J. and Hakes, T.: Tensor Permittivity and Collision Frequency of Plasma. Ohio State Univ. Res. Foundation, R. F. Proj. 941, 3 July 1960.
29. Shkavovsly, I. P., et al: Collision Frequency Associated with High Temperature Air and Scattering Cross-Sections of the Constituents. In same as (9), 24-46.
30. Spitzer, L.: Physics of Fully Ionized Gases. Interscience Publ. Ltd. London 1956.
31. Margenau, H.: Conductivity of Plasmas to Microwaves. Phys. Rev., Vol. 109, 6-9, Jan. 1958.
32. Goldstein, L.: Nonreciprocal Electromagnetic Wave Propagation in Ionized Gaseous Media. IRE Trans., Vol. MTT-6, 19-29, Jan. 1958.
33. Goldberg, P. A.: Electrical Properties of High-Altitude Ionized Shock Waves. 245-260 in Plasma Physics, Ed. by James Drummond, Mc Grav Hill, 1961.
34. Tischer, F. J.: Propagation-Doppler Effects in Space Communications. Proc. IRE, Vol. 48, 570-574, April 1960.
35. Schelkunoff, S. A.: Electromagnetic Waves, Van Nostrand, Princeton, New Jersey 1957.
36. Saxon, D. S.: Modified WKB Methods for the Propagation and Scattering of Electromagnetic Waves. Symp. Elmag. Theory, University of Toronto, 1959.
37. Brenner, H.: Propagation of Electromagnetic Waves. Encyclopedia of Physics, Vol XVI, Springer-Verlag 1958.

38. Huber, P. W.: Theoretical Shock-Layer Plasma Flow Properties for the Slender Probe and Comparison with Flight Results. Second Plasma Sheath Symposium, Boston, Mass., 1962.
39. Lin, S. C.: A Rough Estimate of the Attenuation of Telemetering Signals Through the Ionized Gas Envelope Around a Typical Re-Entry Missile. AVCO Everett, Res. Rep. 74, 1956.
40. Langberg, E. et al: Radiation and Propagation of Telemetry Signals During Hypersonic Re-Entry. Proc. IRE, Symp. on Telemetry, 1958.
41. Tischer, F. J.: Wave Propagation Through Ionized Gas in Space Communications, IAS - Report 59-34, 1959.
42. Taylor, W. C.: Analysis of Radio Signal Interference Effects Due to Ionized Layer Around a Re-Entry Vehicle. Same as (9), 1-9, 1961.
43. Huber, P. W. and Ellis, M. C.: Radio Transmission Through the Plasma Sheath around a Lifting Re-entry Vehicle. NASA TN D-507.
44. Sims, T. E.: Measurement of VHF Signal Attenuation and Antenna Impedance During the Ascending Flight of a Slender Probe at Velocities up to 17,800 Feet per Second. Second Plasma Sheath Symp. Boston, Mass., 1962.
45. Lin, S. C., et al: Radio Echoes from the Ionized Trails Generated by a Manned Satellite during Re-Entry.. AVCO Everett, Res. Rep. 127, 1962.

SUMMARY

Evaluation of approximate relations for the attenuation of signals by the plasma sheath at re-entry shows that the maximum electron density within the shock layer in front of the antenna is the most critical quantity on which the "blackout" time primarily depends. A simplified flow-field model for the shock layer permits computation of the electron density at this location as a function of altitude and velocity for the re-entry trajectory. These data, in turn, permit determination of the approximate "blackout" duration.

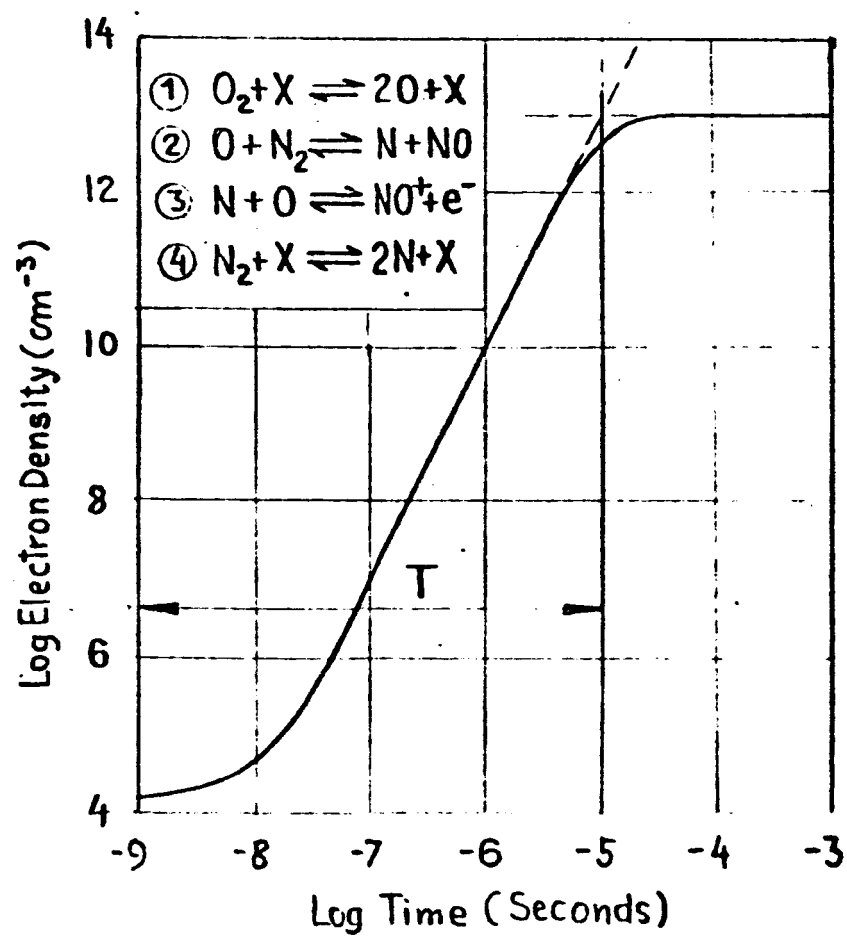


Fig. 1 Electron density versus available reaction time with four reactions. (GE)

(M. H. Bortner (11))

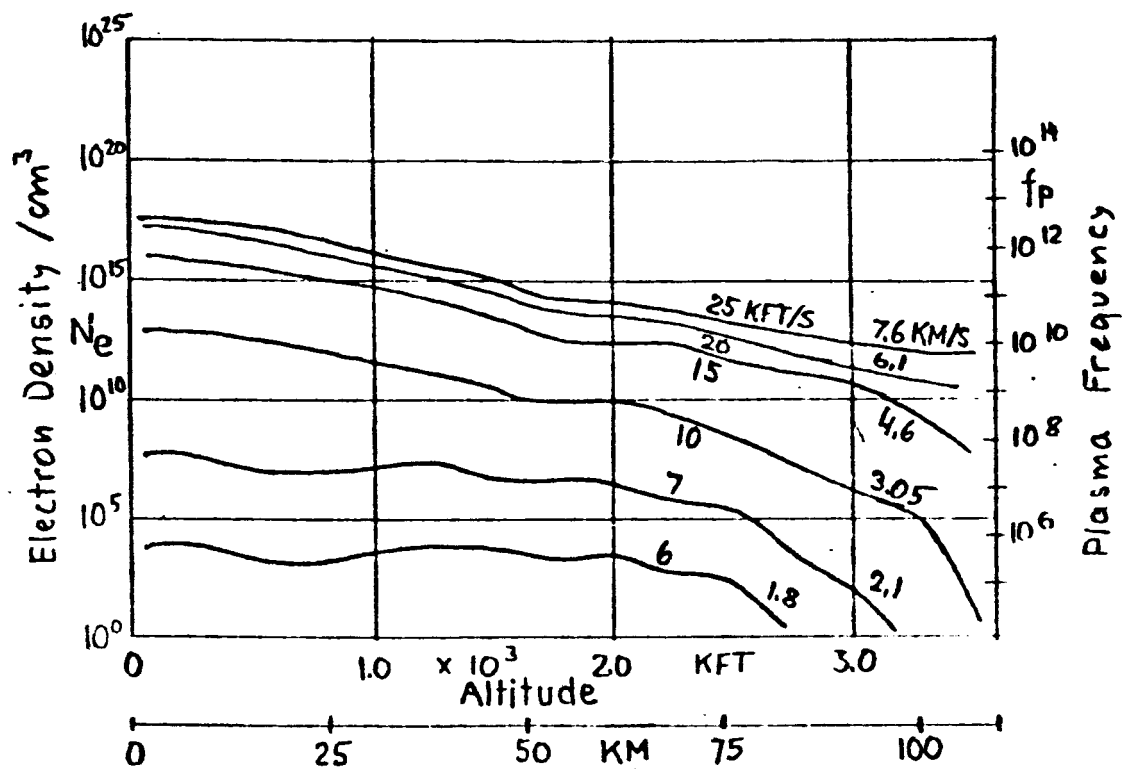


Fig. 2

Electron density and plasma frequency
behind a normal shock versus altitude
and velocity of the re-entry body
(Sisko and Fiskin (27))

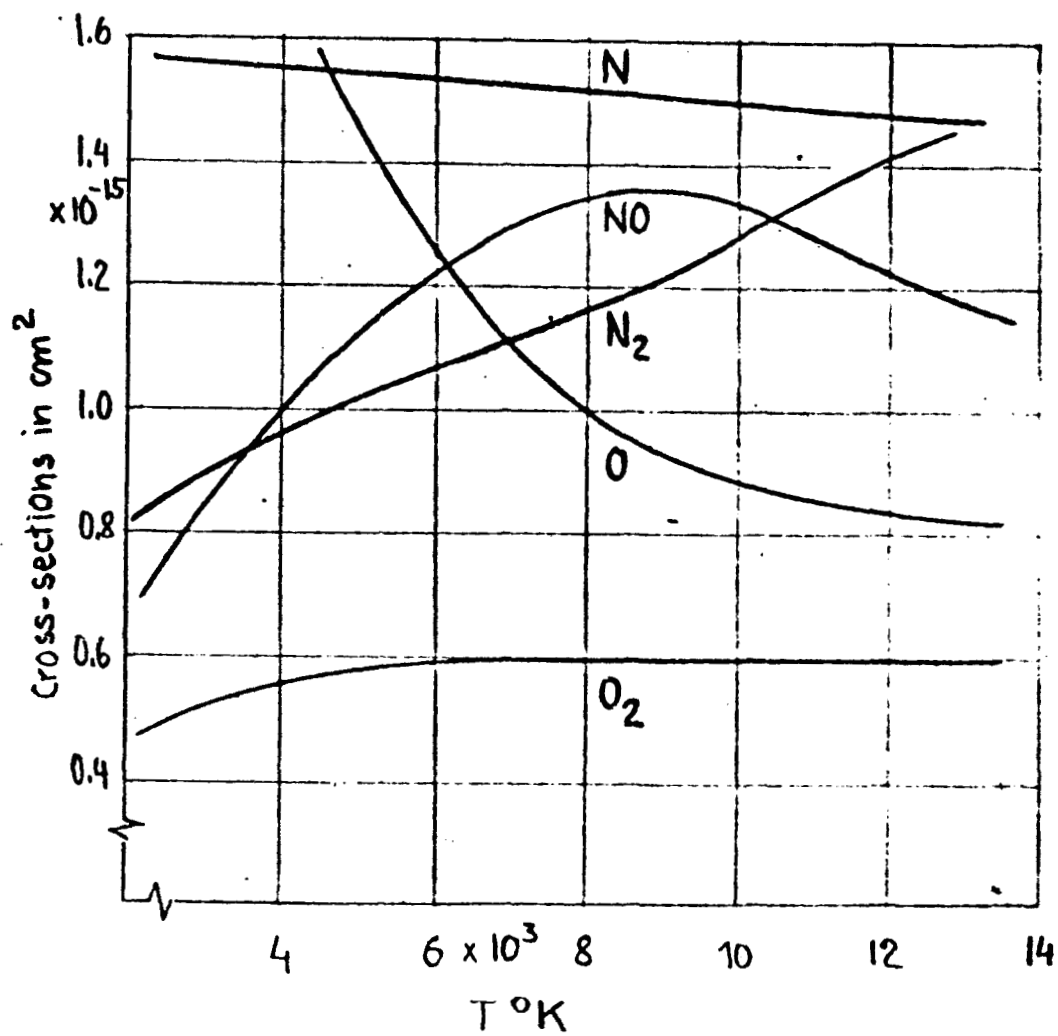


Fig. 3 Collision cross-sections of components of high-temperature air.

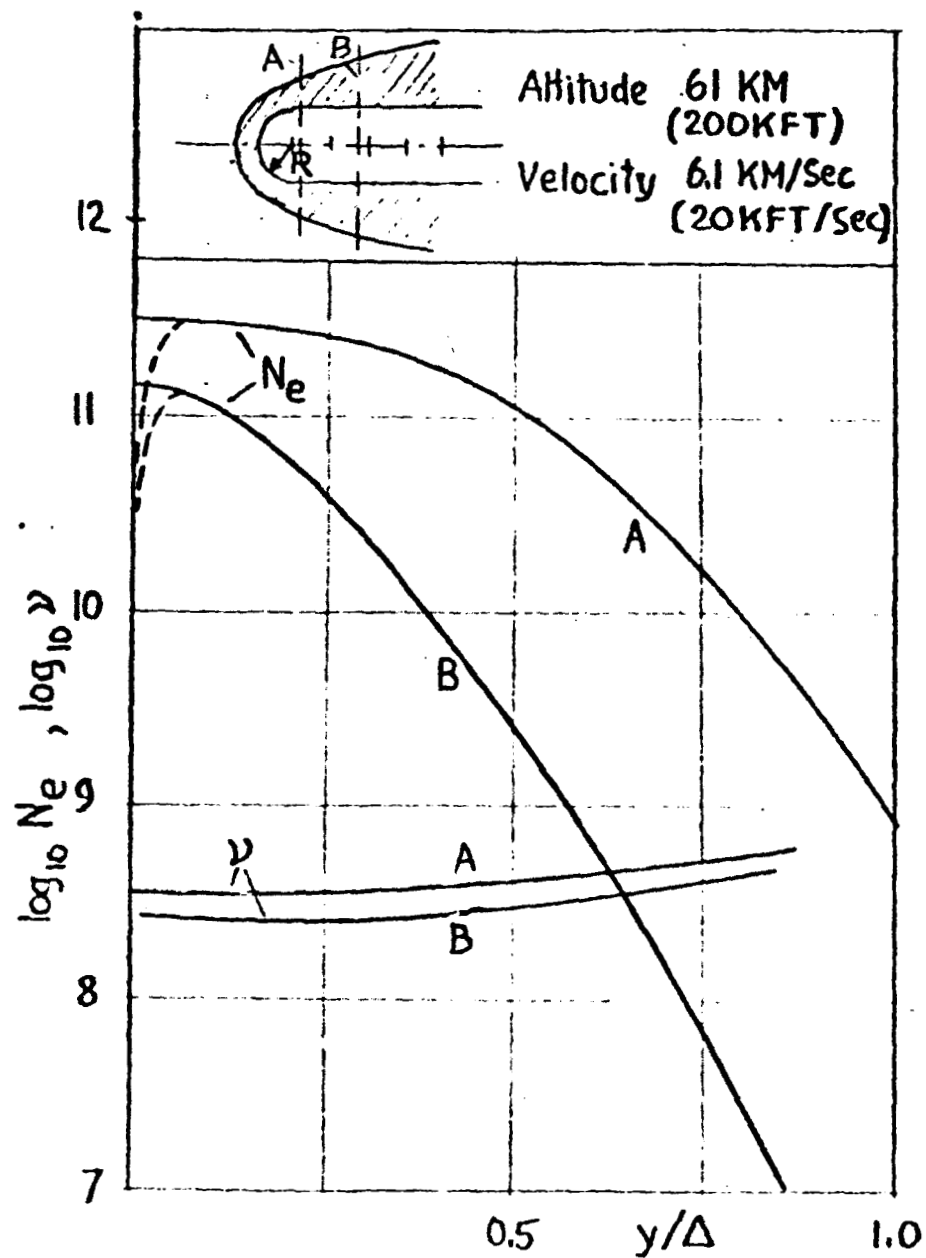


Fig. 4 Distribution of electron density and collision frequency across shock layer of thickness Δ .

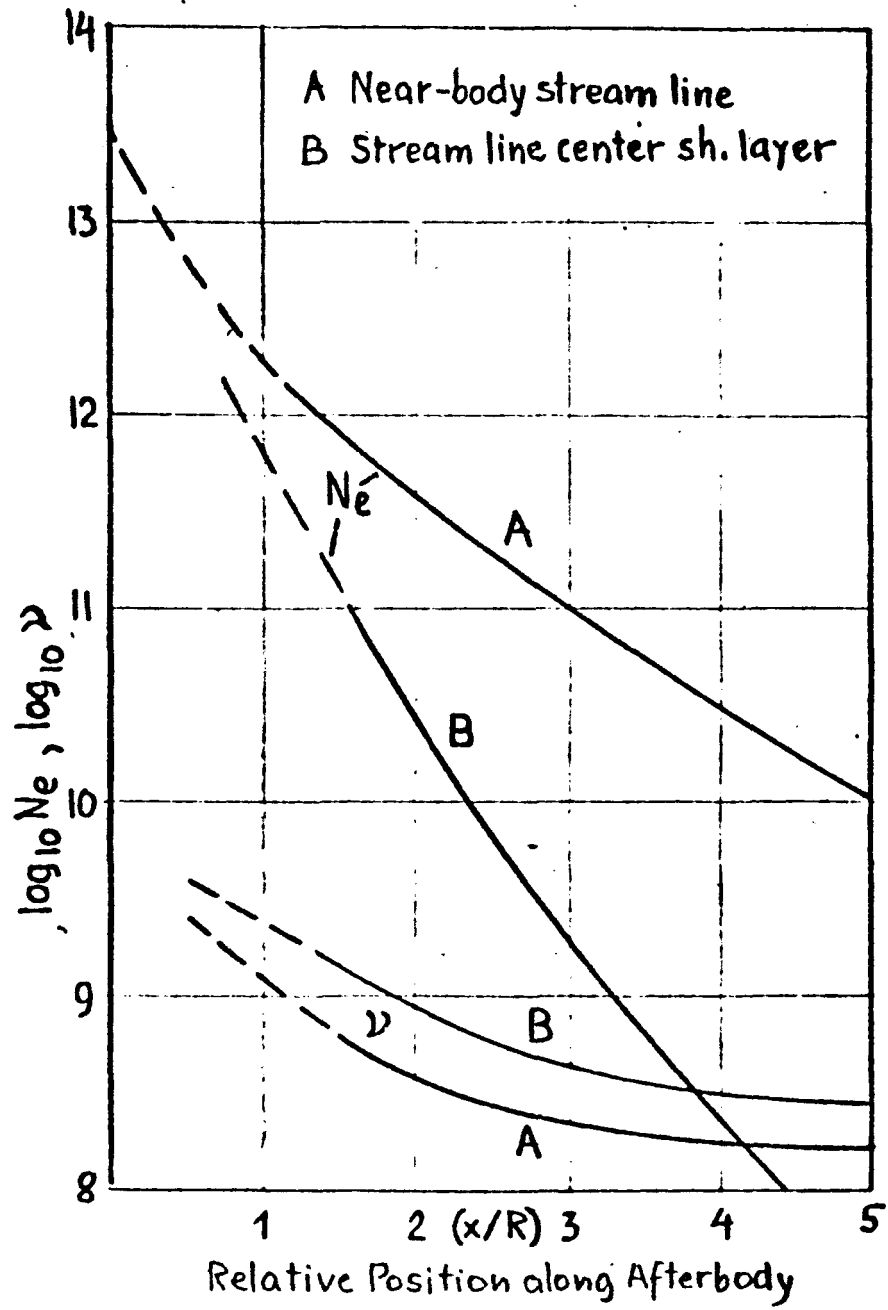


Fig. 5 Distribution of electron density and collision frequency along two stream lines

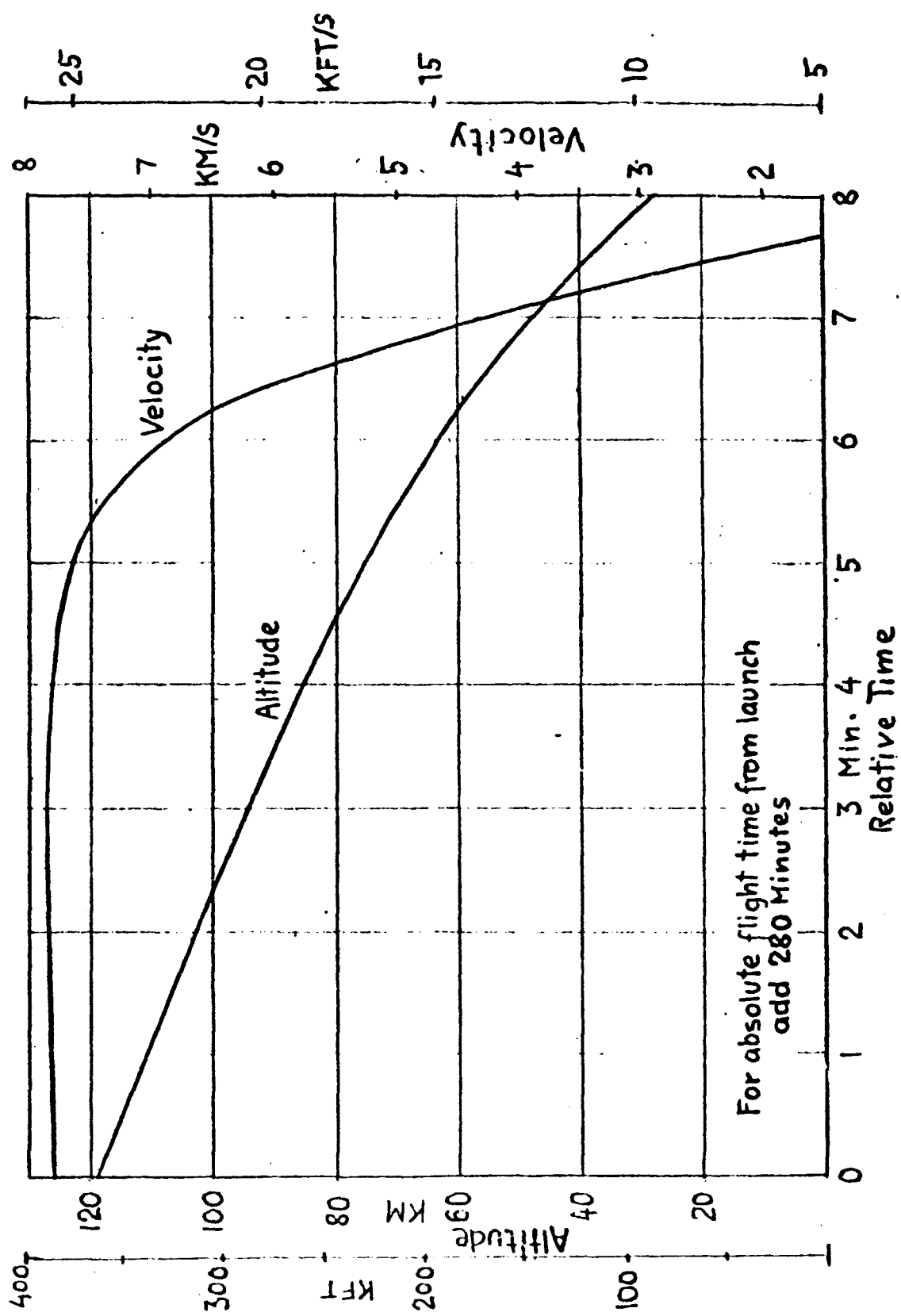


Fig. 6 Trajectory data of the MA-6 Mercury flight.

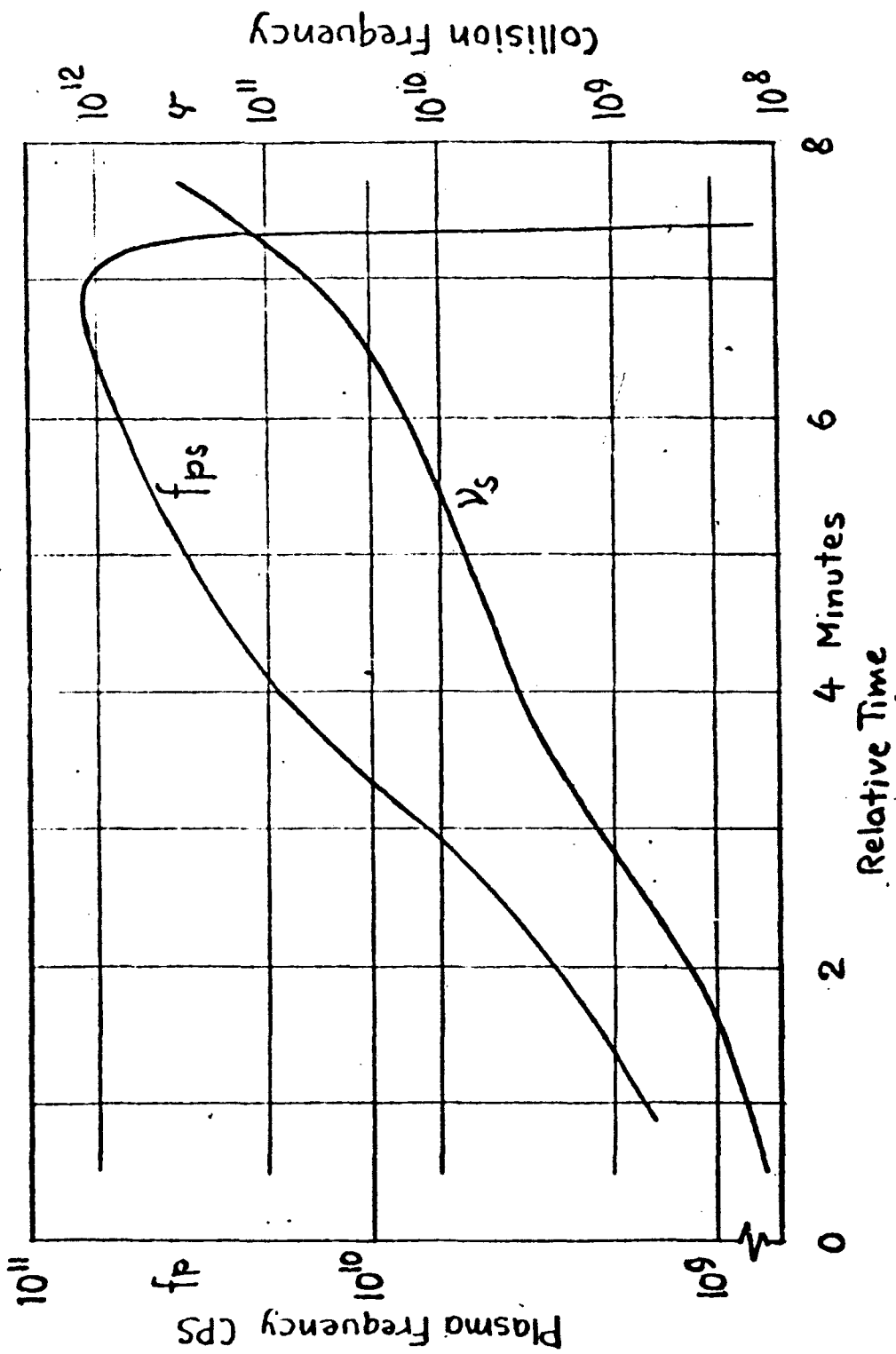


Fig. 7 Plasma and collision frequency behind normal shock along re-entry trajectory

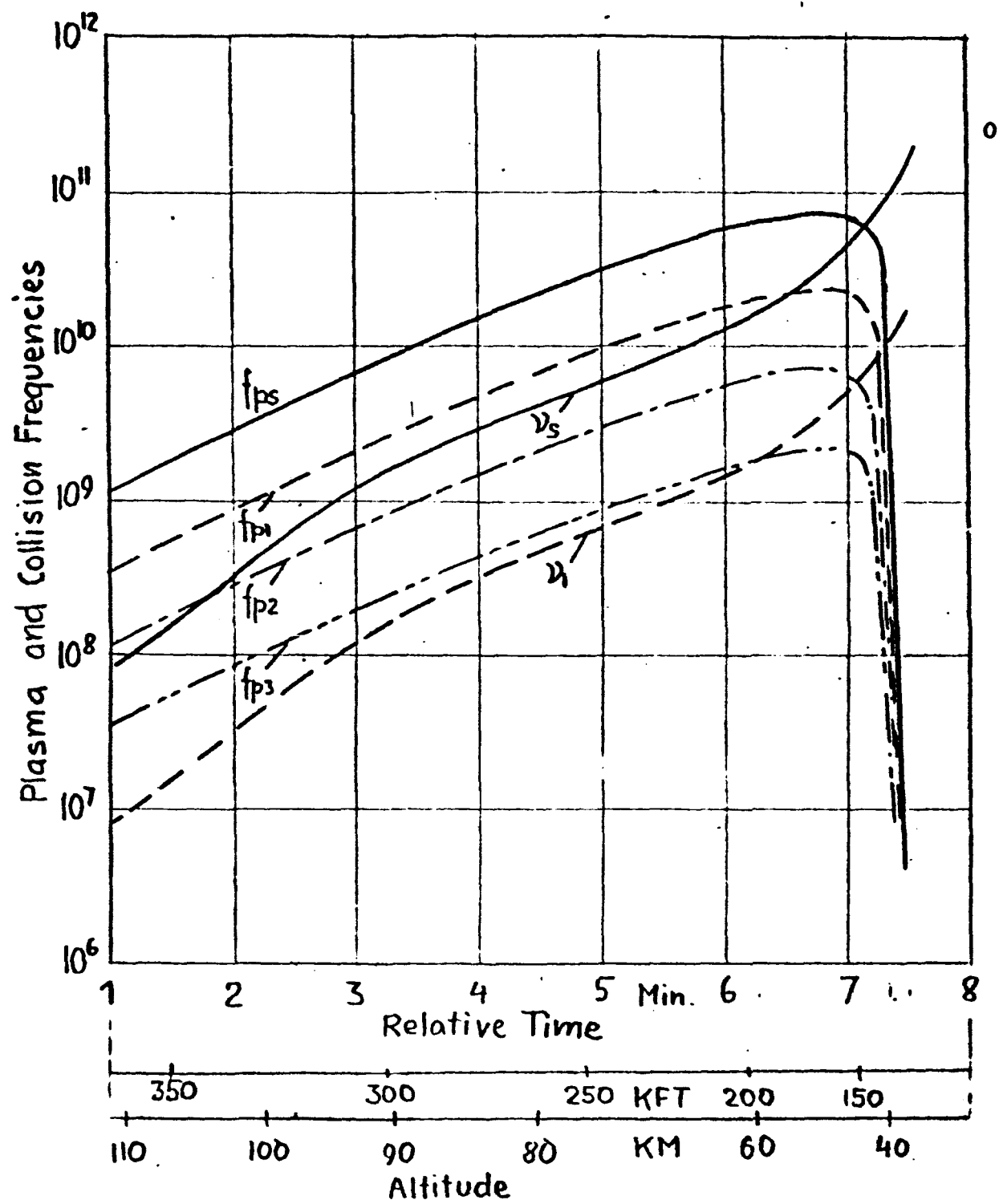


Fig. 8 Plasma and collision frequencies in flow field near the after-body

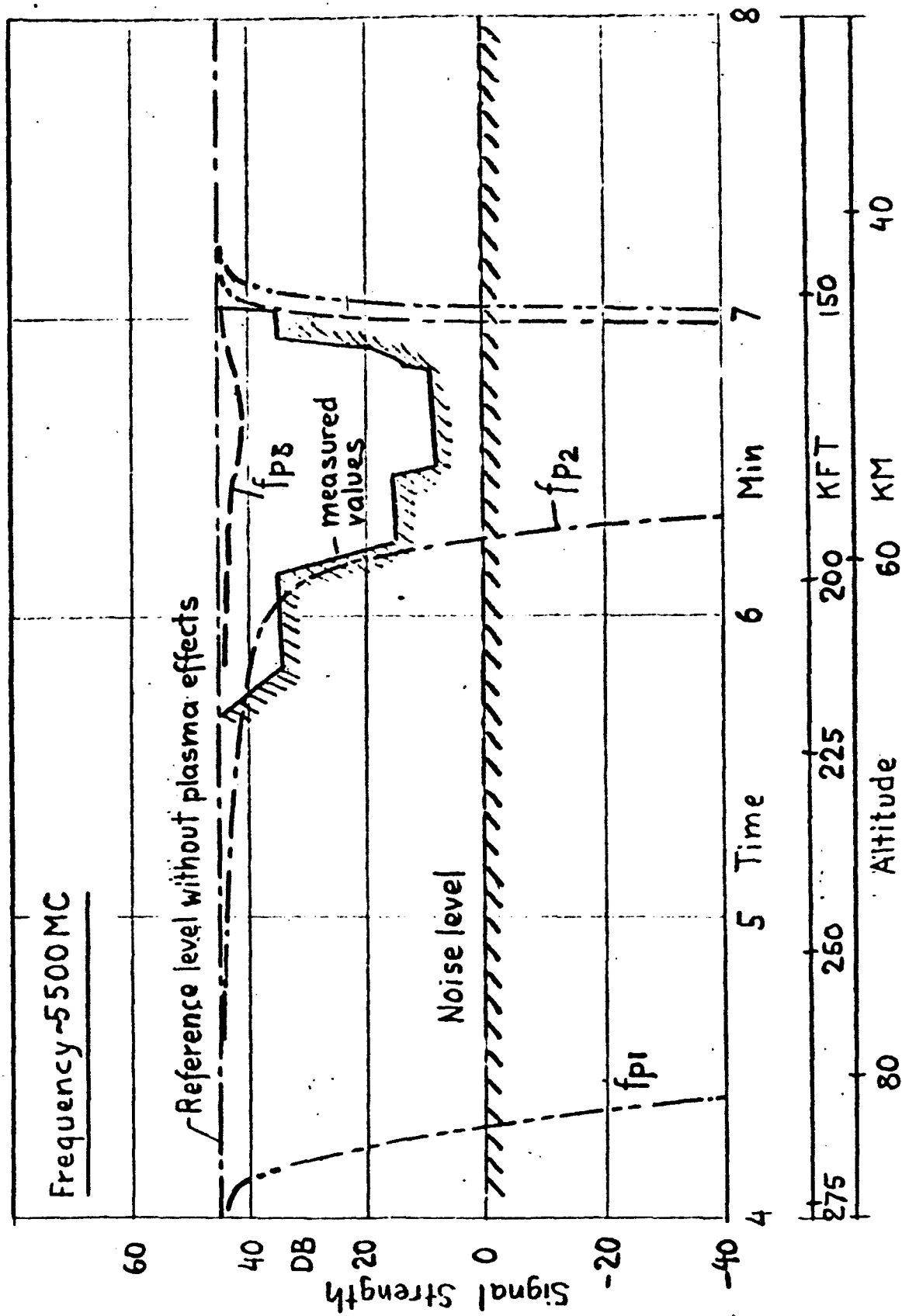


Fig. 9 Relative signal strength for three values of the geometry factor compared with measured values.

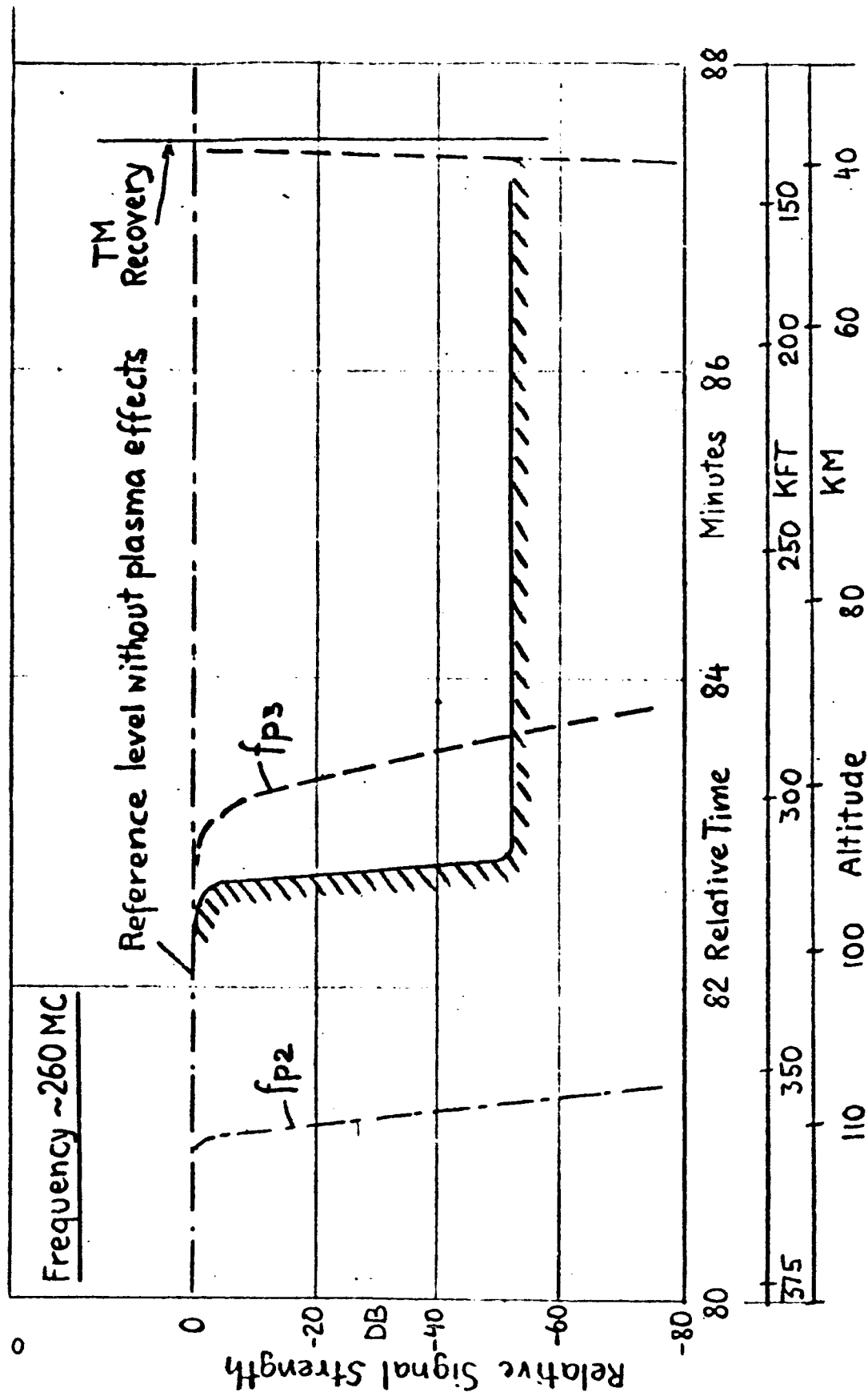


Fig. 10 Relative signal strength for two values of the geometry factor compared with measured values.

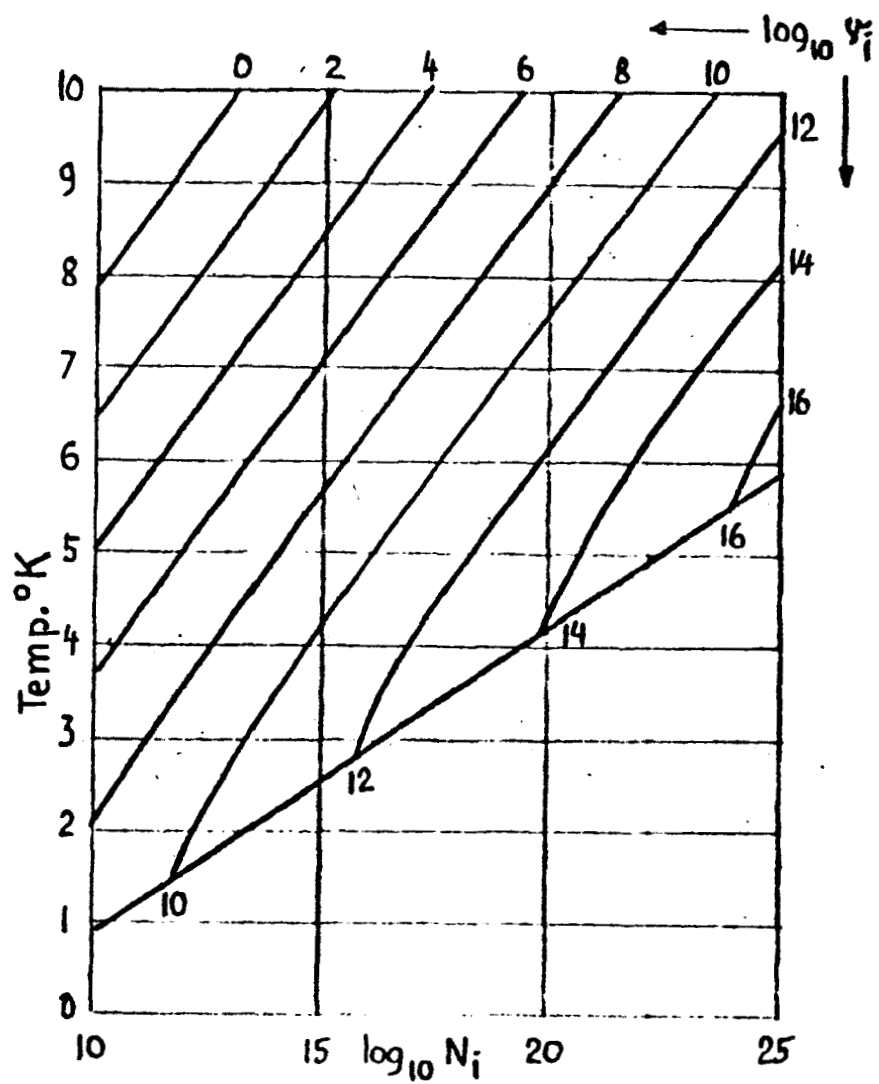


Fig. 11 Collision frequency versus ion density and temperature (Delcroix)